Proceedings of ISFOG 2025
5TH INTERNATIONAL SYMPOSIUM ON
FRONTIERS IN OFFSHORE GEOTECHNICS
Nantes, France | June 9-13 2025

ISBN 978-2-85782-758-0

Effect of sand liquefaction on the first natural frequency of a monopile-supported offshore wind turbine using a non-linear three-dimensional finite element model

*K. Dib
Saint-Joseph University, Beirut, Lebanon

Ph. Alkhoury
Formerly Nantes University, Ecole Centrale Nantes, CRNS, GeM, UMR 6138 F-44600 Saint Nazaire, France

A.-H. Soubra
Nantes University, Ecole Centrale Nantes, CRNS, GeM, UMR 6138 F-44600 Saint Nazaire, France

F. Kaddah
Saint-Joseph University, Beirut, Lebanon

*kassem.dib@net.usj.edu.lb/ Kassem.Dib@univ-nantes.fr

ABSTRACT: Monopile-supported Offshore Wind Turbines (OWTs) are dynamically-sensitive structures and their foundations must be designed with special consideration for cyclic/dynamic loading conditions, especially in seismic regions. The most significant effect of earthquake loads on OWTs is the possible liquefaction at the construction site. Indeed, liquefaction may affect the dynamics of the OWT and particularly its first natural frequency (FNF). This paper aims to investigate the change in the FNF of an OWT-soil system during an earthquake and its subsequent evolution (recovery) using three-dimensional (3D) non-linear finite element (FE) simulations. A 3D FE model of a monopile-supported DTU 10 MW OWT was developed using the PLAXIS3D simulation platform, focusing on homogeneous saturated sands with varying densities (loose, medium and medium dense). The well-established SANISNAD-MS bounding surface plasticity model was adopted in this work to simulate the hydro-mechanical behavior of the sand. The build-up of excess pore water pressure in the soil surrounding the monopile and its effect on the FNF of the OWT-soil system was investigated. The numerical results have shown that the liquefaction in loose, medium, and medium dense sands significantly affects the FNF of an OWT-soil system and induces notable excitation in the soil's natural frequency.

Keywords: Offshore wind turbine, Liquefaction, Natural frequency, Excess pore water pressure, Numerical simulations.

1 INTRODUCTION

Offshore wind turbines (OWTs) have been considered one of the most important sources of renewable energy in recent decades. However, their dynamic sensitivity makes their structural resistance to dynamic loads a significant challenge, particularly in ensuring that their first natural frequency (FNF) remains far from the exciting frequencis (1P, 3P, wind and wave loads). In earthquake-prone regions, seismic loads are critical due to their broad frequency content, which can pose a higher risk of OWT resonance. In addition, sand liquefaction probably leads to a drop in the system FNF potentially shifting it into the 1P excitation frequency range. Despite the importance of this phenomenon, only a limited number of studies have been conducted in this area. In this regard, Demirci et al. (2022) studied the impact of soil liquefaction on the FNF of a 65kW offshore wind turbine. In their study, they proposed a simplified analytical procedure to estimate the changes in the system FNF due to liquefaction. They modeled the tower and monopile using beam elements in SAP2000, while the liquefied and non-liquefied soils were represented by spring elements. The springs for the liquefied soil were based on the work of Dash et al. (2017). Möller et al. (2023) investigated the effect of liquefaction on the elongation of the fundamental period of a 5MW OWT. In their study, they demonstrated that liquefaction could cause a drop in the natural frequency of the whole OWT structure and they highlighted higher excitations of the second

bending modes of the tower. Patra and Haldar (2018) explored the effect of various parameters such as earthquake magnitude and pile length-to-diameter ratio on the response of OWT structures. In their work, OpenSees software was used and the PDMY02 soil constitutive model was adopted. These authors demonstrated that as earthquake magnitude increases, the FNF drops and shifts towards the 1P frequency excitation range.

All the above-mentioned studies focused primarily on the liquefaction stage and did not address the post-liquefaction effects. However, Kementzetzidis et al. (2018) explored this gap by examining the influence of sand liquefaction due to sudden storm loads on the variation of the FNF of an 8MW OWT using the SaniSand soil constitutive model. In their work, they explored several loading scenarios and demonstrated that the foundation stiffness degradation due to sudden storm loads is not permanent and that this degradation dissipated following the post-consolidation of the sand.

In this study, a three-dimensional finite element model of a DTU 10MW OWT embedded in a Karlsruhe quartz sand was developed using PLAXIS 3D software. The bounding surface plasticity model SaniSand-MS was used to accurately represent the dynamic behavior of the Karlsruhe sand. It is important to note that this study does not investigate the effect of the memory surface on the results, which represents a limitation of the current work. Three different sand relative densities (Dr) of 35%, 42% and 52% were considered. The Alkion earthquake, recorded at a rocky site and available from the Cyprus University website, was applied at the bottom of the soil domain without the need of deconvolution process. The evolution of the FNF during both the earthquake and post-earthquake stages was studied and discussed. Notice that wind and wave loads were not considered in this analysis as we are only focusing on the drop of the FNF following earthquake-induced soil liquefaction and its subsequent recovery after consolidation.

2 THREE-DIMENSIONAL NUMERICAL MODEL

Figure 1 shows the developed 3D model where a half-model was used to reduce the computational time. In this paper, the soil medium was represented with the SANISAND-MS constitutive model, implemented as a User-Defined Soil Model in PLAXIS. The monopile and tower were made from steel with a linear elastic behavior.

2.1 Soil domain

The entire soil domain was chosen to have dimensions of 80 m in length, 40 m in width and 75 m in depth as shown in figure 1. This 75m depth comprises 70m of SANISAND-MS soil (indicated in green color) resting atop a 5m layer of linear elastic non-porous rock at the bottom. The inclusion of this rock layer serves to enhance numerical stability as recommended by the Plaxis3D reference manual (2023). Notice that the adopted soil domain dimensions are in accordance with those provided by Eslami and Ghorbani (2022).

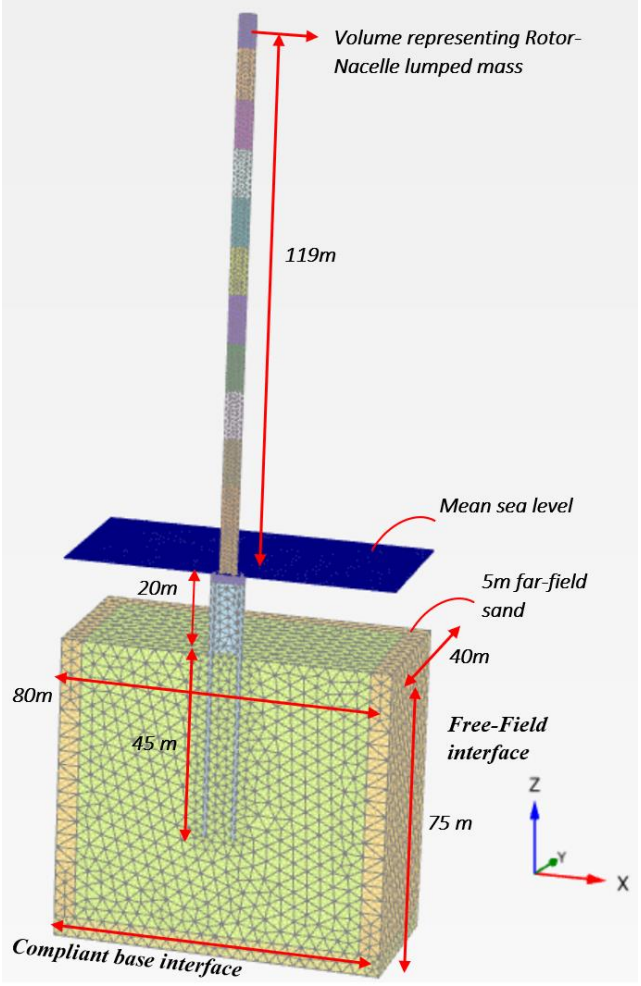

Figure 1.3D model of the studied system.

A 5 m thick far-field surrounding sand zone (indicated in beige color in Figure 1) was considered in the numerical model. This zone was modeled using an elastic perfectly plastic material obeying the Mohr-Coulomb (MC) failure criterion to prevent numerical issues that may arise from the direct contact between the SANISAND-MS soil and the free-field interface implemented in Plaxis3D. The inclusion of a peripheral Mohr-Coulomb (MC) layer is recommended by the PLAXIS 3D manual. This is

because the Free-Field boundary is designed to absorb the input waves by dissipating the stress increments at the boundary. Simple elastic or elasto-plastic materials in direct contact with the Free-Field interface can easily capture these stress increments. In contrast, when using the SaniSand-MS model, the stress increments are calculated in a more complex manner, which can lead to numerical challenges and instabilities. The water depth was assumed to be 20 m above the mudline. The parameters used for the SANISAND-MS soil constitutive model are given in Seequent SANISAND-MS UDSM (2023) while the parameters of the (MC) constitutive model were obtained through numerical simulations of laboratory tests conducted using the *SoilTest* module in Plaxis3D, based on the SANISAND-MS soil parameters of the used Karlsruhe quartz sand. The parameters for both models were shown in Tables 1 and 2 below. As mentioned before, the bedrock layer was modeled as linear elastic non-porous rock. It has an assumed Young modulus of 21,000 MPa and a Poisson ratio of 0.2. The saturated unit weight of the sand was 18.5 kN/m³ while the unit weight of the bedrock was 24 kN/m³. To facilitate rapid soil consolidation after an earthquake, a constant hydraulic conductivity of 0.001 m/s was assumed in all directions. This assumption was made to simplify the model and reduce computational time, although it may influence the results. This may represent a limitation of the study and should be considered in future work.

2.2 OWT structure

The studied structure is 10MW DTU OWT, where geometric parameters are detailed in Alkhoury et al. (2022). The monopile and tower were modeled using volume elements in Plaxis3D. According to the previous reference, the monopile had a total length of 65m, with 8.3m and 8.12m internal and external diameters respectively, and a wall thickness of 9cm. To simplify the model and enhance the numerical stability, the monopile was modeled using a constant diameter pipe section having an outer diameter of 8m and a wall thickness of 1m. The elastic modulus and density were adjusted to ensure that the resulting flexural rigidity (EI) and mass remained consistent with those of the actual section. The pile-soil interface was assumed to be rigid and its stiffness degradation is considered by the degradation of soil shear strength during cyclic earthquake loading. To account for monopile-water interaction, the added mass approach was applied by increasing the steel density. The tower and transition piece were divided into 10 sections, each with a 4 m outer diameter and a 1 m wall thickness. Additionally, a cylindrical steel volume was added at the top of the tower to represent the mass of the rotor-nacelle assembly.

Table 1. Parameters of the SANISAND-MS model for Karlsruhe-Quartz sand.

Parameter	Value
G_0	110
ν	0.05
M_c	1.27
c	0.712
λ_c	0.049
e_0	0.845
ξ	0.27
m	0.01
h_0	5.95
c_h	1.01
n^b	2
A_0	1.06
n^d	1.17
μ_0	260
ζ	0.0005
β	1
e_{ini}	varies
e_{max}	0.874
e_{min}	0.577
$M^{b,max}$	2

Table 2. Mohr-Coulomb parameters for far-field soil

Parameter	Value
E'_{ref}	100000 (kPa)
ν	0.3
c'_{ref}	1 (kPa)
φ'	33°
ψ	8°

2.3 Damping

In this paper, the soil damping was considered through the hysteretic cycles implemented in the soil constitutive model. No additional soil hysteretic damping was considered in the analysis. For the monopile and tower, appropriate values of mass and stiffness Rayleigh damping coefficients (α and β) were used based on the natural frequencies and damping ratios. They are selected based on the interval of values given by Bhattacharya (2018) as follows: 0.23% for hydrodynamic damping, 1.19% for structural damping depending on the type of connections in the structure, resulting in a total damping ratio of 1.42%. No aerodynamic damping was considered as the wind loads are omitted in this study. The corresponding Rayleigh damping coefficients are $\alpha = 0.033$ and $\beta = 0.00336$.

2.4 Calculation steps and boundary conditions

To perform the dynamic analysis, four calculation phases were defined. In phase 1, a gravitational

acceleration was applied to the 3D soil domain to accomplish geostatic equilibrium. In phase 2, the weight of the whole OWT was applied. The boundary conditions (BCs) for this phase and the previous phase were set with fully fixed deformation at the bottom of the soil medium, and a normal restraint on the lateral surfaces. The calculation type for this phase was "plastic" with all water flow boundaries open. In phase 3, a nonlinear dynamic analysis was performed where the OWT was subjected to the earthquake load for 25 seconds. It is important to note that PLAXIS uses a fixed time step. To ensure numerical stability, a maximum time step of 0.002s was initially selected at the start of each calculation step and was subsequently reduced as needed to meet convergence requirements. An implicit time integration scheme, along with the Picos multicore iterative solver, was used during this process. The accelerogram corresponding to the Alkion earthquake was applied at the bottom of the elastic bedrock layer in the X-direction. Figure 2 shows the X-component accelerogram of the Alkion earthquake (University of Cyprus website). During this phase, the water flow BCs were closed at all boundaries except for the top of the soil medium (mudline). The dynamic BCs were set as follows: (1) a compliant base at the bottom of the soil medium to ensure that reflected waves from the layer above are absorbed, (2) free-field BCs on the two lateral faces normal to the X-axis to prevent wave reflection into the soil medium and (3) horizontal fixation in Y-direction applied at the two lateral faces normal to Y-axis. The calculation type for this phase was "Dynamic with consolidation" based on the u-p formulation, as described in the PLAXIS 3D Reference Manual (2023). In phase 4 named “free vibration and consolidation phase”, the earthquake loading is stopped while the structure continued to vibrate freely for 10 seconds, allowing excess pore water pressures in the soil to dissipate through consolidation. Water flow BCs remained open at all boundaries, and the dynamic BCs were maintained as in the previous phase.

2.5 Mesh

The mesh size was selected based on a sensitivity analysis. The maximum element size was set to 3.6m in the far-field following the same procedure outlined by Kuhlemeyer and Lysmer (1973), with additional refinement in vicinity of the monopile soil interface to enhance accuracy in that region. The elements used are based on u-p formulation that considers the stress in the solid skeleton of the soil as well as the accumulation and dissipation of excess pore water pressure. This approach will provide an accurate degradation of element stiffness due to the buildup of excess pore water pressure. The total number of nodes and elements are respectively 54,264 and 29,688.

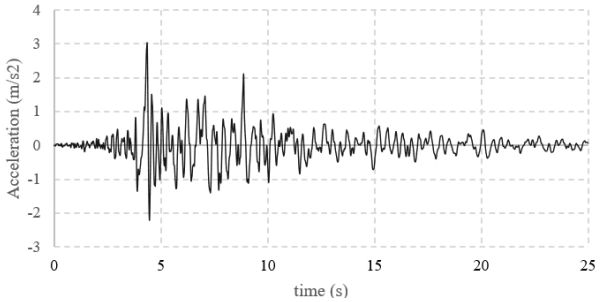

Figure 2. X-component of Alkion earthquake accelerogram (University of Cyprus website).

3 NUMERICAL RESULTS

Calculations were conducted on a 12th Gen Intel® Core ™ i7-12800HX CPU operating at 2.00 GHz. Three simulations were performed, each with a different initial void ratio [relative density (Dr)]: (i) e_{ini} = 0.72 where Dr = 52% (medium dense sand), (ii) e_{ini} = 0.75 where Dr=42% (medium sand) and (iii) e_{ini} = 0.77 where Dr=35% (loose sand). Indeed, Seequent (2023) has shown that the constitutive model parameters reliably capture element test data across the range of examined void ratios/densities.

In order to determine the FNF of the OWT-soil system, in low soil strain conditions, a free decay test was firstly conducted followed by a Fourier analysis of the tower top X-displacement time history. This test consists in applying an arbitrary static lateral force at the tower top, which was subsequently removed to allow for free vibration analysis.

Figure 3 shows the frequency content as obtained from the free decay analysis for the cases with 35% and 52% relative density. The results showed that the FNF of the system was f_0 = 0.195 Hz for both relative densities. The FNF of the system for Dr=42% is expected to have the same value as this relative density falls between the two extreme cases of Dr = 35% and 52%.

3.1 Liquefaction assessment

The excess pore water pressure ratio (EPPR) was monitored at various depths near the monopile to assess the degree of liquefaction induced by the Alkion earthquake. Figures 4-6 show the time evolution of the EPPR for each soil type at three distinct control points. These control points are located in the X-direction, 8 m from the monopile outer surface, but at varying depths of 8 m, 15 m, and 25 m below the mudline. The EPPRs, shown in Figures 4-6 indicate that the liquefaction process (EPPR≥0.9 is considered the

threshold for the onset of liquefaction) persists at 8m for the three soil types, and at 15m depth for only the loose and medium sands (Figure 5), while at 25m, liquefaction persists only for loose sand (Figure 6).

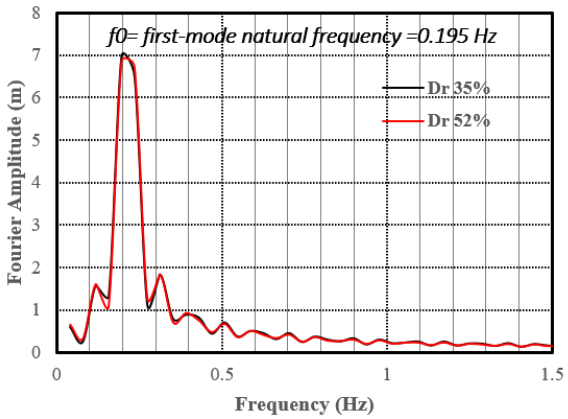

Figure 3. Free decay analysis in frequency domain for the cases of Dr = 35% and Dr = 52% sands.

Following the earthquake, the consolidation process begins, marked by a significant decrease in EPPR (Figures 4-6). The EPPR evolution shows that between 10s and 20s, when the EPPR remains ≥0.9 at 8m and 15m depths (the most affected depths by liquefaction), this period is considered optimal for analyzing the FNF and is referred to in this study as the liquefaction stage (LS). After the earthquake, the EPPR decreases to nearly zero between 27s and 35s at all depths, marking the onset of the consolidation stage (CS).

3.2 First natural frequencies evolution during liquefaction and consolidation stages.

Figures 7–9 present the normalized Fourier amplitudes of the tower top displacement (the time history curves are omitted for brevity). Normalization effectively highlights the dominant frequency by uniformly scaling the amplitudes, which are notably higher during the liquefaction stage compared to the consolidation stage. This method allows for easier identification of the dominant frequencies, minimizing the impact of variations in amplitude magnitudes. The normalization was achieved by dividing all Fourier amplitude values in each stage (LS or CS) by the maximum amplitude value. Aside, three free decay analysis were conducted on soil columns, with relative densities of 35%, 42% and 52%. The results indicated that the fundamental natural frequency of the soil deposit alone (in absence of the OWT structure) is f_{0s}=0.586 Hz. This value is represented in Figures 7-9 by a purple vertical line, alongside a blue vertical line that represents the FNF of the OWT-soil system at low soil strain, as discussed at the beginning of section 3.

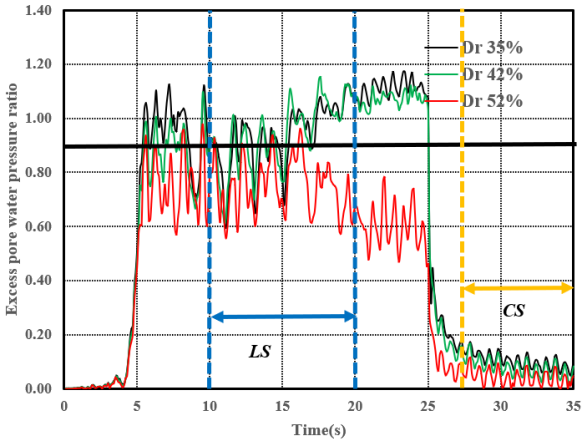

Figure 4. Excess pore water pressure ratio at 8m depth and at 8m away from monopile face.

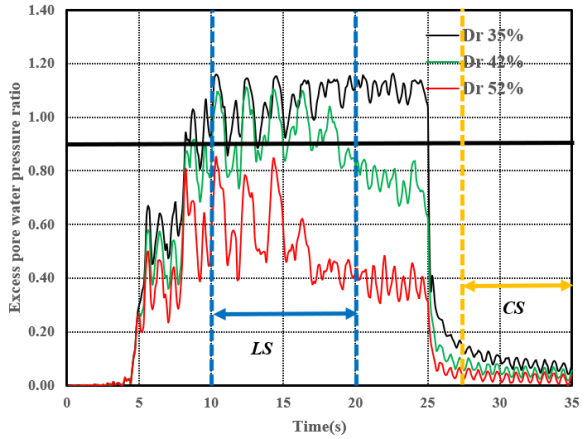

Figure 5. Excess pore water pressure ratio at 15m depth and at 8m away from monopile face

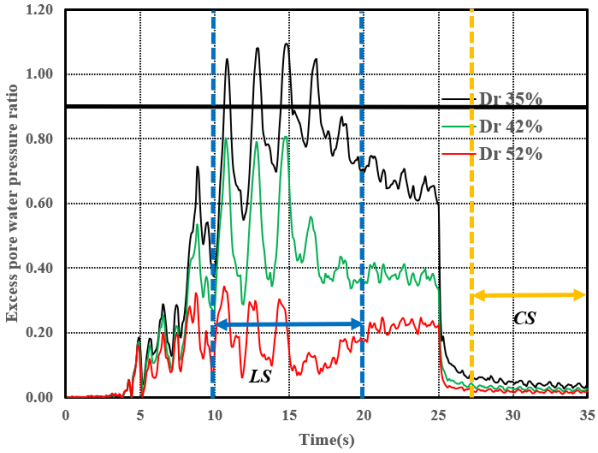

Figure 6. Excess pore water pressure ratio at 25m depth and at 8m away from monopile face.

Figure 10 illustrates the shear stress-shear strain behavior of a soil element located at the control point at 15m depth for each soil relative density during both LS and CS. The dotted lines represent the approximated slope (shear stiffness) of the soil during LS, while the dashed lines are during CS.

From Figures 7-9, it is clear that, during LS (red curves), the FNF of the system dropped from f_0 = 0.195 Hz to f_l = 0.156 Hz (where *l* denotes liquefaction) bringing it closer to 1P load excitation frequencies (0.1Hz-0.16Hz). Following this, the FNF recovered and increased during CS (black curves) from f_l=0.156 Hz to f_c=0.235Hz (where *c* denotes consolidation), appraoching the fixed-base tower FNF. This is interpreted in Figure 10 where all dashed lines (represeting approximated soil shear stiffness during CS) exhibit a steeper slope than the dotted lines (during LS), indicating that the loss of soil shear strength during liquefaction contributes to a decrease in soil lateral resistance and thus in OWT-soil system FNF. It is important to mention here, that the drop in the system's FNF was consistent across all three cases regardless of the extent of soil shear stiffness loss.

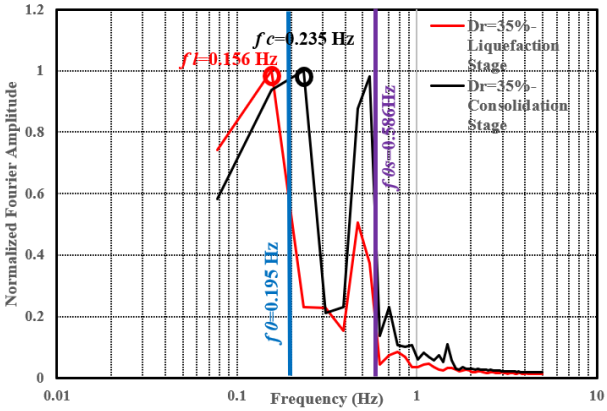

Figure 7. Normalized fourier transform of the tower top displacement during LS and CS for loose sand.

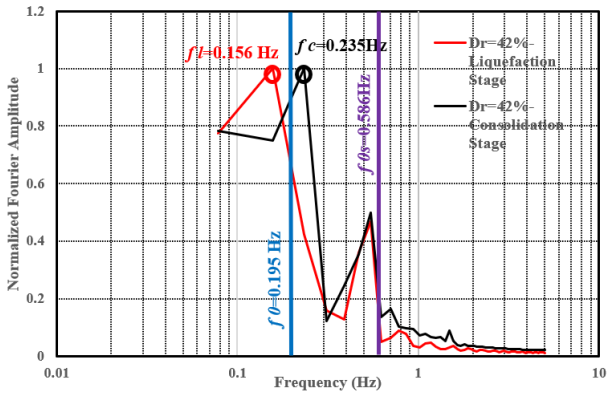

Figure 8. Normalized fourier transform of the tower top displacement during LS and CS for medium sand.

Furthermore, the reduction in the system's FNF was accompanied by an excitation of the soil FNF. During LS, this excitation reached 50% of the system FNF for loose and medium sands (as shown by the red curve in Figures 7 and 8) and 40% of the system FNF excitation in the case of dense sand (Figure 9). This excitation is attributed to the liquefaction process, which transforms the soil into a semi-liquid state, drastically reducing shear stiffness (Figure 10) and soil damping (caused by the absence of friction between sand grains due to excessive pore water pressure), thereby facilitating the excitation of the soil FNF. This soil FNF excitation also results from the interaction between the tower and the soil, where the tower induces vibrations in the soil.

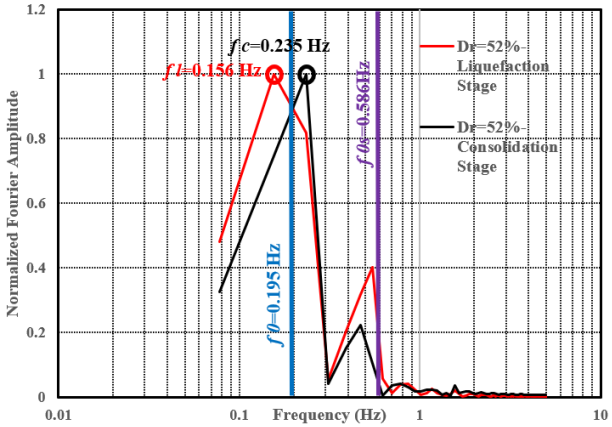

Figure 9. Normalized fourier transform of the tower top displacement during LS and CS for medium dense sand.

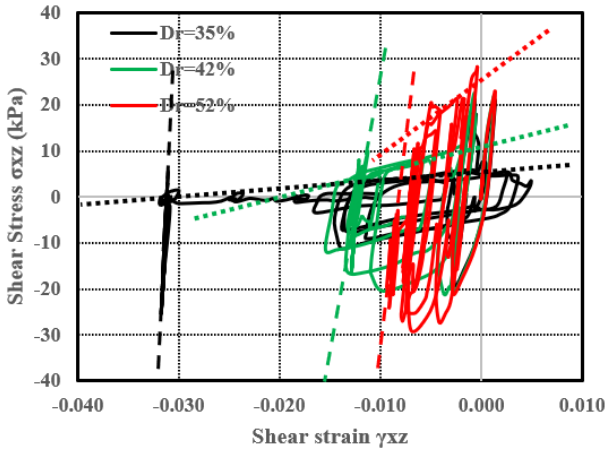

Figure 10. Shear stress- Shear strain behavior of soil element at 15 m depth 8m far from monopile face for three different soil relative densities.

Furthermore, this excitation was observed to increase during CS for loose sand indicating an important vibration energy transfer from the tower to the soil due to their interaction, placing the structure in a state of reduced stability due to multiple high excitation frequencies (0.156 Hz, 0.235 Hz, and 0.546 Hz) as depicted by the black curve in Figure 7. Meanwhile, the soil FNF excitation remained at 50% and decreased to 20% of the system FNF excitation for medium and medium-dense sands, respectively. This indicates a higher absorbtion of the energy transfered from the tower vibrarions to the soil, thereby helping to maintain the structural stability in good condition.

4 CONCLUSION

This study conducted three dimensional finite element (FE) simulations of a 10 MW DTU offshore wind turbine subjected to seismic loads, considering three different relative densities of sand. The results showed that liquefaction in loose, medium, and medium-dense sands led to an approximate reduction of 20% in the system first natural frequency , bringing it closer to the 1P excitation frequencies. After consolidation, the system FNF increased and approached the fixed-base frequency of the OWT structure. Additionally, during liquefaction, the FNF of the soil domain was excited to nearly half of the system‘s FNF excitation. The results also indicated that during consolidation, the soil-tower interaction was particularly pronounced in loose sand, leading to weak stability of the structure, while in medium and medium-dense sands, the interaction was less significant, preserving the structural stability under favorable conditions. In summary, results have shown that liquefaction reduces the first bending mode frequency of the structure due to the loss of soil stiffness and lateral resistance while exciting the soil‘s fundamental mode frequency. After the eathquake, consolidation allows the soil to regain strength, leading to an increase in the system‘s FNF, while the interaction between the structure and the soil remains dynamic. The energy transfer from the turbine to the soil continues, potentially leading to sustained excitaion of the soil fundamental frequency.

Future research could focus on examining various earthquake scenarios with different parameters, assessing the effect of soil permeability based on the void ratio, and validating the finite element model through physical modeling.

AUTHOR CONTRIBUTION STATEMENT

K. Dib: Data curation, Formal Analysis, Writing-Original draft. **Ph. Alkhoury**: Methodology, Supervision, Writing- Reviewing and Editing . **A.-H. Soubra, F. Kaddah**: Conceptualization, Methodology, Supervision, Writing- Reviewing and Editing

ACKNOWLEDGEMENTS

The authors are grateful for the financial support provided by “Conseil de recherche-Université Saint Joseph de Beirut”.

REFERENCES

Alkhoury, Ph., Soubra, A.-H., Rey, V. and Aït-Ahmed, M. (2022). Dynamic analysis of a monopile-supported offshore wind turbine considering the soil-foundation-structure interaction. *Soil Dynamics and Earthquake Engineering*, 158.

Bhattacharya, S. (2018). Design of foundations of offshore wind turbines. *JohnWiley & Sons Ltd*, 2019.

Demirci, H., Jalbi, S., Lombardi, D. and Bhattachrya, S. (2022). Liquefaction effects on the fundamental frequency of monopile supported offshore wind turbines (OWTs). *Bulletin of Earthquake Engineering*, 20: 3359-3384. https://doi.org/10.1007/s10518-022-01360-9

Dash, S., Rouholamin, M., Lombardi, D. and Bhattachrya, S. (2017). A practical method for construction of p-y curves for liquefiable soils. *Soil Dynamics and Earthquake Engineering*, 97: 478-481. https://doi.org/10.1016/j.soildyn.2017.03.002

Eslami, A. and Ghorbani, A. (2022). Seismic response of offshore wind turbines supported on monopiles and suction buckets: Numerical modelling and soft computing study. *Soil Dynamics and Earthquake Engineering*, 159. https://doi.org/10.1016/j.soildyn.2022.107284

Kementzetzidis, E., Versteijlin, W., Nernheim, A. and Pisano, F. (2018). 3D FE dynamic modelling of offshore wind turbines in sand: Natural frequency evolution in the-pre-to after storm transition. *Numerical Methods in Geotechnical Engineering*.

Kuhlemeyer, RL., Lysmer, J. (1973). Finite element method accuracy for wave propagation problems. *J Soil Mech Found Div*, 99(5):421–7.

Moller, J., Kontoe, S., Taborda, D. and Potts, D. (2023). Resonance in offshore wind turbine systems due to seismic loading and extensive soil liquefaction. *10th European Conference on Numerical methods in Geotechnical Engineering*. https://doi.org/10.53243/NUMGE2023-126

Patra, S. and Haldar, S. (2018). Response of monopile supported offshore wind turbine in liquefied soil. *Indian Geotechnical conference.*

Seequent. SANISAND-MS UDSM (2023). PLAXIS 3D.2023.2

Plaxis3D refrence manual (2023)-*Bentley, Geostudio-Plaxis (knowledge base).*

Univeristy of Cyprus. (2002). http://www.eng.ucy.ac.cy/petros/Earthquakes/earthquakes.htm